



Cite this: RSC Adv., 2019, 9, 38047

# Improved light-harvesting and suppressed charge recombination by introduction of a nanograss-like $\text{SnO}_2$ interlayer for efficient CdS quantum dot sensitized solar cells<sup>†</sup>

 Sangaraju Sambasivam,<sup>a</sup> Chandu V. V. Muralee Gopi,<sup>id,\*b</sup> Hee-Je Kim<sup>id,\*b</sup> and Ihab M. Obaidat<sup>\*a</sup>

Quantum dot sensitized solar cell (QDSSC) performance is primarily limited by the recombination of charges at the interfaces of  $\text{TiO}_2$ /quantum dot (QD) sensitizer/electrolyte. Hence, blocking or suppressing the charge recombination is an essential requirement to elevate the QDSSC performance to the next level. To retard the charge recombination, herein, we propose the introduction of a  $\text{SnO}_2$  nanograss (NG) interlayer on the surface of  $\text{TiO}_2$  using the facile chemical bath deposition method. The  $\text{SnO}_2$  NG interlayer not only inhibits the interfacial recombination processes in QDSSCs but also enhances the light-harvesting capability in generating more excitons. Hence, the  $\text{TiO}_2/\text{SnO}_2$  NG/CdS QDSSCs can achieve the power conversion efficiency of 3.15%, which is superior to that of a  $\text{TiO}_2/\text{CdS}$  device (2.16%). Electrochemical impedance spectroscopy, open-circuit voltage decay and dark current analyses confirm that the recombination of charges at the photoanode/electrolyte interface is suppressed and the life time is improved by introducing the  $\text{SnO}_2$  NG interlayer between the  $\text{TiO}_2$  and CdS QD sensitizer.

Received 10th October 2019  
 Accepted 15th November 2019

DOI: 10.1039/c9ra08234d  
[rsc.li/rsc-advances](http://rsc.li/rsc-advances)

## 1. Introduction

Because of the increased environmental pollution and the limited fossil fuels, the demand for renewable and sustainable energy systems, such as solar energy, has increased over the last few decades. Among the different solar energy systems, third-generation solar cells such as quantum dot sensitized solar cells (QDSSCs) are gaining considerable interest owing to their advantages of inorganic structure, high theoretical efficiency, easy fabrication and low-cost.<sup>1,2</sup> Various metal chalcogenide-semiconductors such as CdS, CdSe, PbS,  $\text{CdSe}_x\text{S}_{1-x}$ ,  $\text{CuInS}_2$ ,  $\text{CuInZnS}$ , etc. have been investigated as promising sensitizers for the QDSSCs due to their tunable band gap, high absorption coefficient and multiple exciton generation (MEG).<sup>3-5</sup> A typical structure of the QDSSC is composed of a QD-sensitized  $\text{TiO}_2$  photoelectrode, polysulfide electrolyte ( $\text{S}^{2-}/\text{S}_n^{2-}$ ), and counter electrode, which leads to various hetero-interfaces.<sup>6-8</sup> Although QDs have unique characteristics, the QDSSCs achieved a low power conversion efficiency (PCE = 12%) due to the recombination of charges that occur at the photoanode/QDs/electrolyte

interfaces.<sup>9,10</sup> Hence, considerable attempts have been carried out to suppress the charge recombination, such as the use of a passivation layer on QDs surface, the introduction of metal doping in QDs, and overcoating wide band gap (or insulating) materials over  $\text{TiO}_2$  surface or QDs, which results in the enhanced QDSSCs performance.<sup>11-13</sup>

Recently, Z. Ren *et al.* reported that the application of amorphous  $\text{TiO}_2$  intermediate layer between the interface of QDs and  $\text{ZnS}/\text{SiO}_2$  layer, effectively suppressed the charge recombination and improved the photovoltaic performance.<sup>13</sup> Recently, Li *et al.* developed the effective integration of ultra-high density well-separated ZnO nanocrystals (NCs) homoepitaxially grown on the surface of an individual vertically oriented single-crystalline (SC) ZnO nanoneedle (NN).<sup>14</sup> The fabricated monolithic ZnO NCs-on-NN SC hybrids may hold great promise for enhanced photovoltaic performance (*e.g.*, electron mobility) of ZnO NC-sensitized solar cells. Very recently, Y. S. Lee *et al.* introduced the  $\text{TiO}_2/\text{ZnS}/\text{CdS}/\text{ZnS}$  cascade structure, in which the presence of ZnS intermediate layers are not only capable of retarding the charge recombination but also improve the light-harvesting efficiency, resulting in the enhanced power conversion efficiency (3.69%).<sup>15</sup> Z. Du *et al.* studied the CdSe QDSSCs based on FTO/ $\text{TiO}_2$  without and with  $\text{TiCl}_4$  treatment.<sup>16</sup> The QDSSCs based on FTO/ $\text{TiO}_2/\text{TiCl}_4/\text{CdSe}$  photoanode exhibited higher PCE (5.36%) than the FTO/ $\text{TiO}_2/\text{CdSe}$  (5.11%), which is mainly due to the  $\text{TiCl}_4$  treatment

<sup>a</sup>Department of Physics, United Arab Emirates University, Al-Ain 15551, United Arab Emirates. E-mail: [iobaidat@uaeu.ac.ae](mailto:iobaidat@uaeu.ac.ae)

<sup>b</sup>Department of Electrical Engineering, Pusan National University, Geumjeong-gu, Busan, South Korea-46241. E-mail: [naga5673@gmail.com](mailto:naga5673@gmail.com); [heeje@pusan.ac.kr](mailto:heeje@pusan.ac.kr)

† Electronic supplementary information (ESI) available. See DOI: [10.1039/c9ra08234d](https://doi.org/10.1039/c9ra08234d)



that reduced the recombination of charges at the interface of  $\text{TiO}_2$  and  $\text{CdSe}$  QDs. Very recently, Ozu *et al.* reported  $\text{ZnO}$  nanowire (NW) passivation by an ultrathin  $\text{SnO}_2$  layer, reducing the density of the deep traps by the absorbed oxygen and hydroxyl groups on the  $\text{ZnO}$  NW surface.<sup>17</sup>  $\text{SnO}_2$  passivation not only reduced the surface recombination but also led to an upward shift of the Fermi energy, causing more efficient electron transfer to  $\text{ZnO}$ . Very recently, E. N. Jayaweera *et al.* developed the  $\text{SnO}_2/\text{MgO}$  films for the  $\text{CdS}/\text{ZnS}$  based QDSSCs ( $\text{SnO}_2/\text{MgO}/\text{CdS}/\text{ZnS}$ ) to boost the solar cell performance by efficiently preventing the charge recombination at the interface of  $\text{SnO}_2/\text{sensitizer}$ .<sup>18</sup> As a result, the  $\text{SnO}_2/\text{MgO}/\text{CdS}/\text{ZnS}$  QDSSC achieved a PCE of 1.33%. Therefore, the idea of deposition of wide band-gap semiconductor materials on the surface of semiconductor nanoparticles could effectively improve the QDSSC performance.

Motivated from the recent results of hindering the charge recombination at the  $\text{TiO}_2/\text{QDs}/\text{electrolyte}$  interfaces, herein, we propose the introduction of a novel  $\text{SnO}_2$  nanograss (NG) interlayer on  $\text{TiO}_2$  surface *via* a simple chemical bath deposition (CBD) route. The deposition of  $\text{SnO}_2$  NG between the  $\text{TiO}_2$  and  $\text{CdS}$  QDs suppresses charge recombination, resulting in enhanced QDSSC performance. Further, the photoanode of  $\text{TiO}_2/\text{SnO}_2$  NG/CdS achieves improved light-harvesting and also provides efficient charge transport. The QDSSCs based on  $\text{TiO}_2/\text{SnO}_2$  NG/CdS photoelectrode showed an impressive PCE of 3.15% under one sun illumination, which was much higher than that with  $\text{TiO}_2/\text{CdS}$  photoelectrode (2.16%). The achieved high efficiency by  $\text{SnO}_2$  NG interlayer signifies an important approach to further elevate QDSSCs performance to the next level.

## 2. Experimental section

### 2.1. Materials

Tin chloride dihydrate ( $\text{SnCl}_2 \cdot 2\text{H}_2\text{O}$ ), hexamethylenetetramine (HMTA,  $\text{C}_6\text{H}_{12}\text{N}_4$ ), cadmium acetate dihydrate ( $\text{Cd}(\text{CH}_3\text{COO})_2 \cdot 2\text{H}_2\text{O}$ ), sodium sulfide ( $\text{Na}_2\text{S}$ ), sulfur (S) and potassium chloride (KCl) were obtained from Sigma-Aldrich Co., South Korea and used as such without purification.  $\text{TiO}_2$  paste (Ti-nanoxide HT/SP) was supplied by Solaronix.

### 2.2. Preparation of $\text{TiO}_2/\text{SnO}_2$ NG/CdS photoelectrode

Prior to the deposition, the fluorine-doped tin oxide (FTO,  $13 \Omega \text{sq}^{-2}$ ) glasses ( $1.3 \times 1.5 \text{ cm}^2$ ) were well washed with acetone, ethanol and deionized (DI) water for 10 min each. Mesoporous

$\text{TiO}_2$  electrodes were prepared using doctor-blading a  $\text{TiO}_2$  paste (20 nm diameter, Solaronix SA) onto FTO substrate and then the samples were maintained at  $450^\circ\text{C}$  for 30 min. Then,  $\text{SnO}_2$  NG was grown on the  $\text{TiO}_2$  surface *via* a facile CBD reaction. In detail, 0.05 M  $\text{SnCl}_2 \cdot 2\text{H}_2\text{O}$  and 0.15 M HMTA were mixed in 70 mL DI water under magnetic stirring for 30 min. The as-prepared  $\text{TiO}_2$  samples were dipped horizontally into the  $\text{SnO}_2$  growth solution and heated at  $95^\circ\text{C}$  for 10 h. The HMTA in precursor solution not only serves as a surfactant by reducing the surface tension between the growth solution and substrate, but also it supports the growth of  $\text{SnO}_2$  layer. After deposition, the  $\text{SnO}_2$  NG loaded FTO/ $\text{TiO}_2$  films were rinsed with DI water and ethanol, and then heated at  $450^\circ\text{C}$  for 30 min. The as-fabricated electrodes are termed the  $\text{TiO}_2/\text{SnO}_2$  NG.

Next, the  $\text{CdS}$  QDs were loaded on  $\text{TiO}_2/\text{SnO}_2$  NG by a facile successive ionic layer adsorption and reaction (SILAR) method. Briefly,  $\text{TiO}_2/\text{SnO}_2$  NG films were dipped in aqueous 0.1 M  $\text{Cd}(\text{CH}_3\text{COO})_2 \cdot 2\text{H}_2\text{O}$  solution for 5 min, rinsed with ethanol; then dipped in aqueous 0.1 M  $\text{Na}_2\text{S}$  solution for 5 min, and then once again rinsed with ethanol. Such a process is called one SILAR cycle and a totally 8 SILAR cycles were repeated. The as-obtained films are termed the  $\text{TiO}_2/\text{SnO}_2$  NG/CdS. The schematic of the fabrication process of  $\text{TiO}_2/\text{SnO}_2$  NG/CdS on FTO substrate is shown in Fig. 1.

### 2.3. Counter electrode and QDSSC device fabrication

$\text{CuS}$  counter electrodes were prepared on FTO substrates using CBD method following our previous report.<sup>19</sup> Finally, the QDSSCs were sandwiched with as-fabricated  $\text{TiO}_2/\text{SnO}_2$  NG/CdS photoelectrodes and  $\text{CuS}$  counter electrodes by a sealant (SX 1170-60, Solaronix) and polysulfide electrolyte containing of 1 M  $\text{Na}_2\text{S}$ , 2 M S and 0.1 M KCl in methanol and water solution (7 : 3).

### 2.4. Characterization and measurements

The crystalline phase, elemental analysis and morphology of the electrodes were investigated using X-ray diffraction (XRD, D/Max-2400), X-ray photon spectroscopy (XPS, VG Scientific ESCALAB 250) and scanning electron microscope (SEM, S-2400, Hitachi) with energy-dispersive X-ray spectroscopy (EDX, 15 kV) mapping characterizations, respectively. The optical absorption properties of the as-prepared electrodes were analyzed by UV-visible absorption spectra (OPTIZEN 3220UV). The photocurrent-voltage ( $J-V$ ) measurements were conducted by an ABET Technologies (USA) solar simulator, which can exhibit an

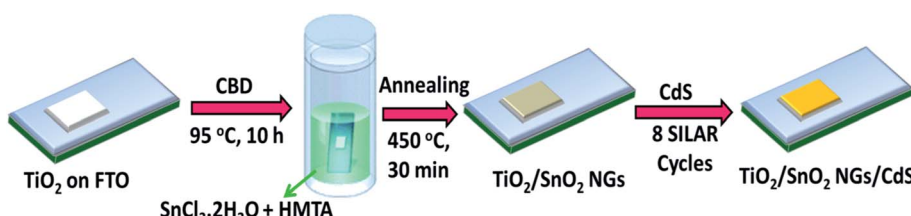


Fig. 1 The schematic of the preparation process of  $\text{TiO}_2/\text{SnO}_2$  NG/CdS on FTO substrate.

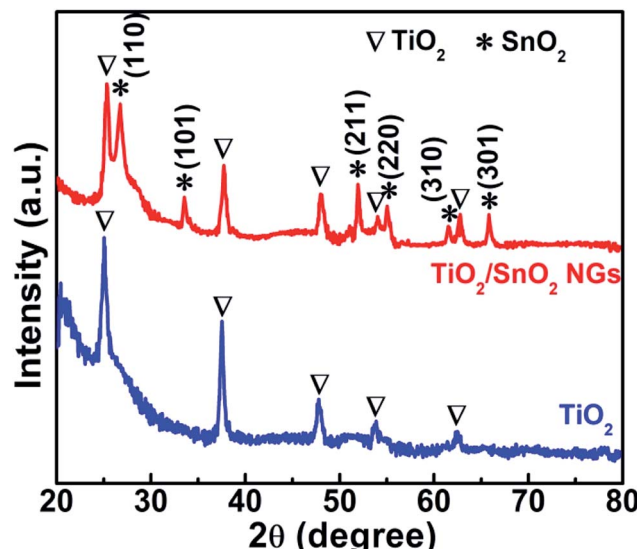


Fig. 2 XRD patterns of  $\text{TiO}_2$  and  $\text{TiO}_2/\text{SnO}_2$  NG on FTO substrate.

intensity of  $100 \text{ mW cm}^{-2}$ . Electrochemical impedance spectroscopy (EIS) was carried out by a SP-150 BioLogic station with a frequency range of  $500 \text{ kHz}$  to  $0.1 \text{ Hz}$  and AC amplitude of  $10 \text{ mV}$ .

### 3. Results and discussion

#### 3.1. Structural and morphological characterization

Facile and cost-effective CBD method was used to grow the  $\text{SnO}_2$  NG interlayer onto the  $\text{TiO}_2$  surface. Initially, the crystalline structure of the  $\text{TiO}_2$  and  $\text{TiO}_2/\text{SnO}_2$  NG electrodes was investigated using XRD characterization. The XRD patterns of the as-prepared  $\text{TiO}_2$  and  $\text{TiO}_2/\text{SnO}_2$  NG are depicted in Fig. 2. As seen in Fig. 2, both the  $\text{TiO}_2$  and  $\text{TiO}_2/\text{SnO}_2$  NG samples exhibit peaks at  $2\theta = 25.1^\circ, 37.5^\circ, 47.8^\circ, 53.9^\circ$  and  $62.3^\circ$ , which are well-matched with the  $\text{TiO}_2$  tetragonal anatase structure (JCPDS: 21-1272). After the deposition of  $\text{SnO}_2$  over  $\text{TiO}_2$  surface, new diffraction peaks are observed at  $2\theta = 26.7^\circ, 33.6^\circ, 51.9^\circ, 54.9^\circ, 61.5^\circ$  and  $65.8^\circ$ , which are well-consistent with the  $\text{SnO}_2$  tetragonal structure (JCPDS: 41-1445).<sup>20</sup>

XPS characterization was performed to investigate the valence states of elements in  $\text{TiO}_2/\text{SnO}_2$  NG electrode. The XPS survey spectra of  $\text{TiO}_2/\text{SnO}_2$  NG sample is shown in Fig. 3a, which clearly shows the presence of only Ti, Sn, O and C elements. The presence of carbon element in the total survey scan spectrum is ascribed to the exposure of air sample to air. As depicted in Fig. 3b, the XPS spectrum of Ti 2p, exhibits the  $\text{Ti } 2\text{p}_{3/2}$  and  $\text{Ti } 2\text{p}_{1/2}$  peaks that are centered at  $458.7$  and  $464.5 \text{ eV}$ , respectively. These spectra are consistent with the presence of  $\text{Ti}^{4+}$  valence state. Due to the spin-orbit

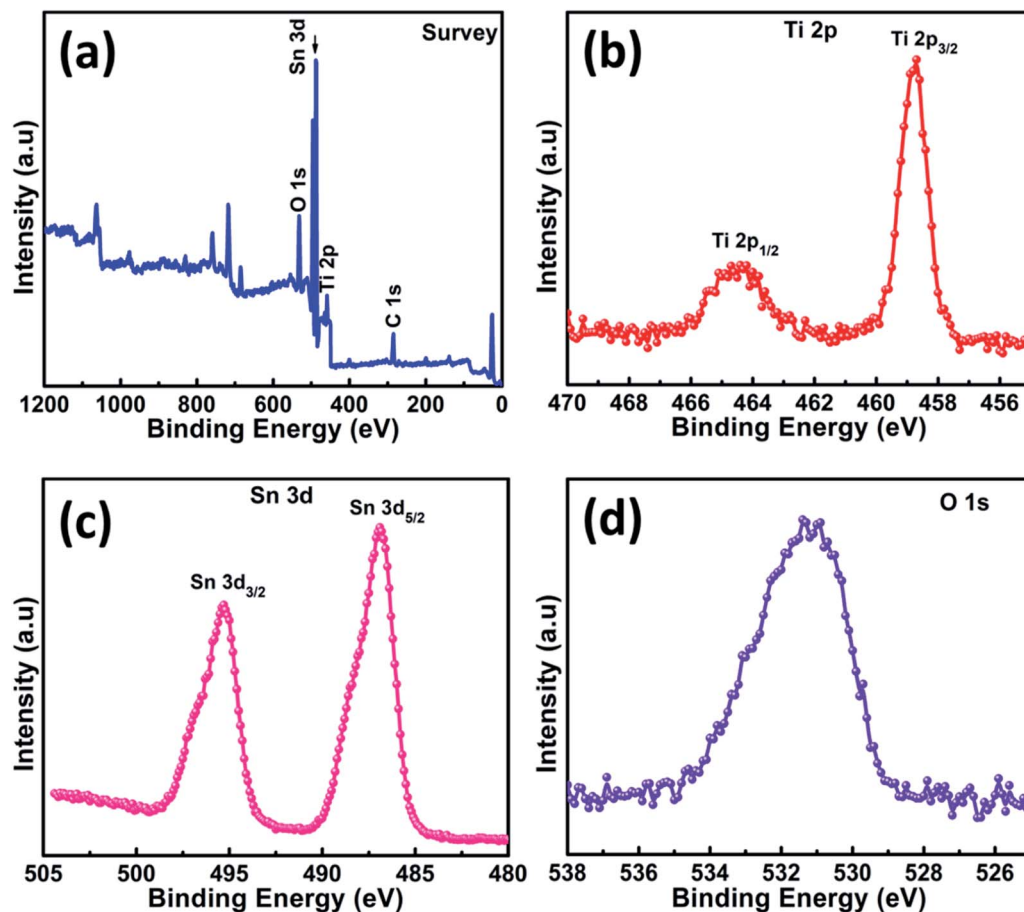


Fig. 3 (a) XPS survey spectra and high-resolution XPS spectra of (b) Ti 2p, (c) Sn 3d and (d) O 1s in  $\text{TiO}_2/\text{SnO}_2$  NG sample.



coupling of Ti 2p, the obtained peaks are separated by 5.8 eV.<sup>21</sup> The Sn 3d spectrum presented in Fig. 3c exhibited two peaks at 486.8 eV and 495.3 eV which are indexed to Sn 3d<sub>5/2</sub> and Sn 3d<sub>3/2</sub>, respectively, and agree with the Sn<sup>4+</sup> state in SnO<sub>2</sub>.<sup>22</sup> As depicted in Fig. 3d, the spectrum of O 1s displays a peak that is centered at 530.9 eV, corresponding to O<sub>2</sub> in the TiO<sub>2</sub> and SnO<sub>2</sub> crystal lattices.<sup>22,23</sup> The XRD and XPS results confirmed the formation of SnO<sub>2</sub> NG on the TiO<sub>2</sub> surface.

The surface morphologies of the as-prepared TiO<sub>2</sub> and TiO<sub>2</sub>/SnO<sub>2</sub> NG electrodes were studied by SEM analysis, and the corresponding images are depicted in Fig. 3a and b for TiO<sub>2</sub> on FTO substrate, and in Fig. 4c and d for SnO<sub>2</sub> onto the TiO<sub>2</sub> surface (TiO<sub>2</sub>/SnO<sub>2</sub>) NG. As shown in Fig. 4a, the TiO<sub>2</sub> nanoparticles are uniformly distributed throughout the substrate. It can be clearly seen from Fig. 4b, that the TiO<sub>2</sub> exhibits spherical nanoparticle morphology with diameter in the range of ~16 to ~20 nm. CBD method was used to grow the SnO<sub>2</sub> nanostructures on the surface of TiO<sub>2</sub>. It can be clearly observed in Fig. 4c, that the SnO<sub>2</sub> exhibits the nanograss (NG) morphology. The diameter of the SnO<sub>2</sub> NG was estimated to be in the range of ~21 to ~46 nm (Fig. 4d). The SEM images clearly reveal that the SnO<sub>2</sub> NG nanostructures were successfully grown on TiO<sub>2</sub> surface. In addition, SEM-EDX color mapping was carried out to examine the distribution of elements in the TiO<sub>2</sub>/SnO<sub>2</sub> NG. The mapping images shown in Fig. S1† clearly revealed the homogeneous distribution of Ti, Sn and O elements in the as-prepared TiO<sub>2</sub>/SnO<sub>2</sub> NG electrode.

### 3.2. Optical properties

UV-vis absorption measurements were carried out to demonstrate the optical properties of the TiO<sub>2</sub>, TiO<sub>2</sub>/SnO<sub>2</sub> NG, TiO<sub>2</sub>/CdS and TiO<sub>2</sub>/SnO<sub>2</sub> NG/CdS samples and the results are plotted in Fig. 5 in the range of 300 to 800 nm. The TiO<sub>2</sub> sample exhibits the absorption edge at around 378 nm. The growth of SnO<sub>2</sub> NG on TiO<sub>2</sub> surface increased the absorption intensity. In addition, the absorption onset of TiO<sub>2</sub>/SnO<sub>2</sub> NG increased to 388 nm. The

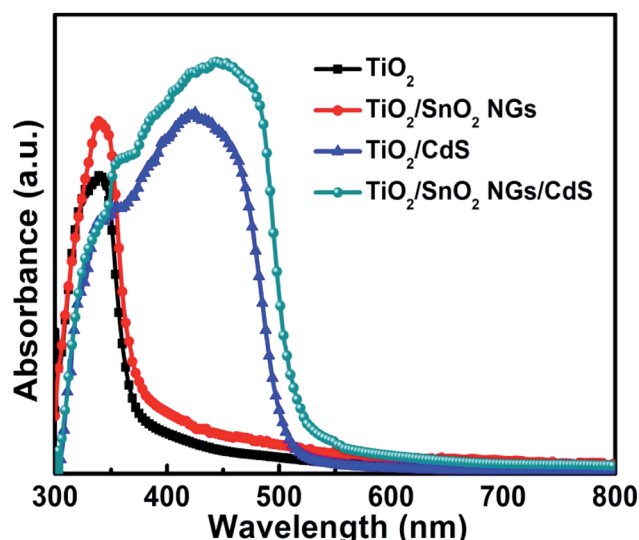


Fig. 5 UV-vis absorption spectra of as-prepared electrodes.

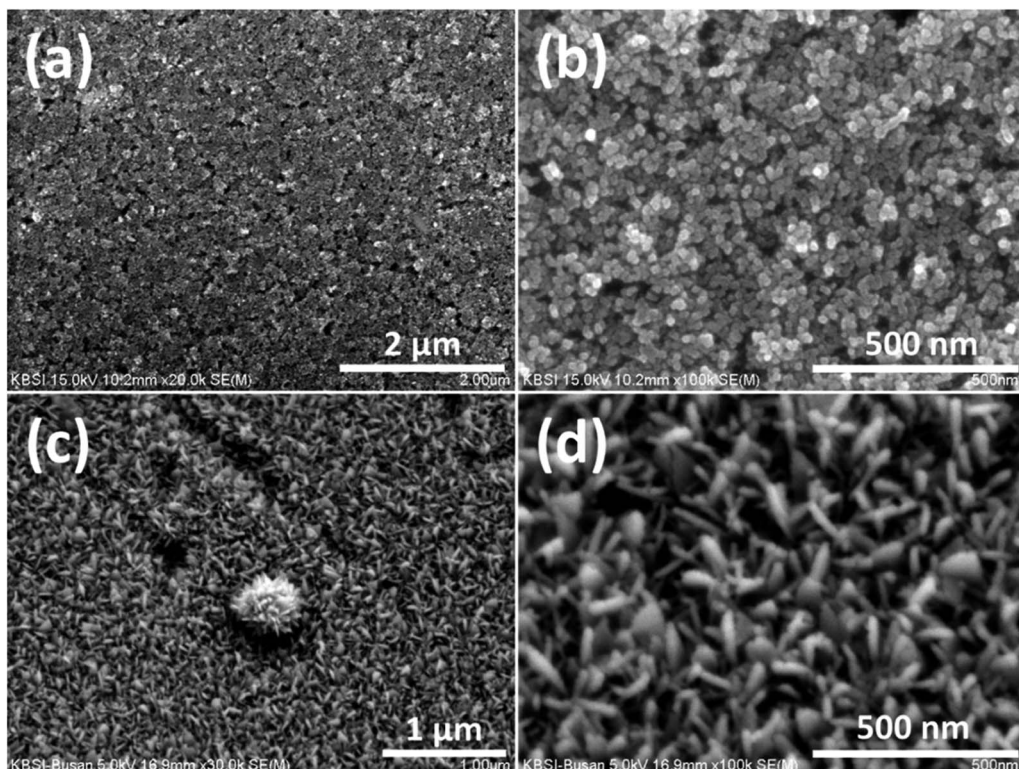


Fig. 4 SEM images of (a and b) TiO<sub>2</sub> and (c and d) TiO<sub>2</sub>/SnO<sub>2</sub> NG on FTO substrate at different magnifications.

absorption onsets of the  $\text{TiO}_2/\text{CdS}$  and  $\text{TiO}_2/\text{SnO}_2$  NG/CdS samples were measured to be 510 nm and 525 nm, respectively. The absorption onset of the  $\text{TiO}_2/\text{SnO}_2$  NG/CdS electrode was increased and with higher absorbance compared to  $\text{TiO}_2/\text{CdS}$ . These observations can be attributed to the growth of  $\text{SnO}_2$  NG passivation/barrier layer over  $\text{TiO}_2$  surface. Also, the  $\text{SnO}_2$  NG interlayer supports the nucleation and growth of CdS QDs, which results in the high rate absorption of  $\text{TiO}_2/\text{SnO}_2$  NG/CdS electrode.

### 3.3. Photovoltaic performance and charge transfer of the QDSSCs

To evaluate the impact of the  $\text{SnO}_2$  NG interlayer on the photoanodes, the photovoltaic behaviors of  $\text{TiO}_2/\text{CdS}$  and  $\text{TiO}_2/\text{SnO}_2$  NG/CdS based QDSSCs have been investigated. The  $J-V$  profiles of the as-fabricated QDSSCs were measured under one sun illumination and the related photovoltaic considerations are depicted in Fig. 6a and Table 1. The  $\text{TiO}_2/\text{CdS}$  QDSSC exhibits  $J_{\text{SC}}$  of  $6.64 \text{ mA cm}^{-2}$ ,  $V_{\text{OC}}$  of  $0.614 \text{ V}$ , and FF of 0.530, resulting in a PCE of 2.16%. When a  $\text{SnO}_2$  NG layer was grown on  $\text{TiO}_2$  surface ( $\text{TiO}_2/\text{SnO}_2$  NG/CdS), the  $J_{\text{SC}}$ ,  $V_{\text{OC}}$  and FF were considerably improved to  $8.92 \text{ mA cm}^{-2}$ ,  $0.619 \text{ V}$ , and 0.570, respectively, resulting in the elevated PCE of 3.15%, which is much higher than the PCE of  $\text{TiO}_2/\text{CdS}$  (2.16%) photoelectrode.

The enhanced  $V_{\text{OC}}$  and  $J_{\text{SC}}$  of the  $\text{TiO}_2/\text{SnO}_2$  NG/CdS based QDSSCs are attributed to the reduced charge recombination and the fast charge transfer at the  $\text{TiO}_2/\text{QDs}/\text{electrolyte}$  interfaces. Hence, the PCE of QDSSC has improved from 2.16% to 3.15% by the growth of  $\text{SnO}_2$  NG interlayer over the  $\text{TiO}_2$  surface. Furthermore, incident photon to current conversion efficiency (IPCE) study was carried out to illustrate the light absorption and electron generation behaviors in the QDSSCs. Fig. 6b depicts the IPCE plots of the as-prepared QDSSCs. It is evident from the IPCE spectra that the introduction of  $\text{SnO}_2$  NG interlayer enhanced the IPCE response from 66% to 75% and also enlarged the IPCE response edge from 548 nm to 568 nm. The  $\text{TiO}_2/\text{SnO}_2$  NG/CdS based QDSSCs exhibits higher IPCE response than the  $\text{TiO}_2/\text{CdS}$ , which is in good agreement with the  $J_{\text{SC}}$  of the  $J-V$  plots.

In order to demonstrate the impact of  $\text{SnO}_2$  NG interlayer on the photoelectrode films, EIS measurement was conducted under forward bias ( $V_{\text{OC}}$ ) and illumination. The Nyquist plots of the  $\text{TiO}_2/\text{CdS}$  and  $\text{TiO}_2/\text{SnO}_2$  NG/CdS based QDSSCs are depicted in Fig. 6c. The Nyquist plots of both devices exhibit the two semicircles, in which the first (small) semicircle is obtained in the high-frequency region and represents the charge transfer resistance ( $R_{\text{CE}}$ ), the chemical capacitance ( $C_{\text{CE}}$ ) at the interface of the counter electrode/electrolyte, and the series resistance ( $R_s$ ) which is obtained in the high-frequency region where the

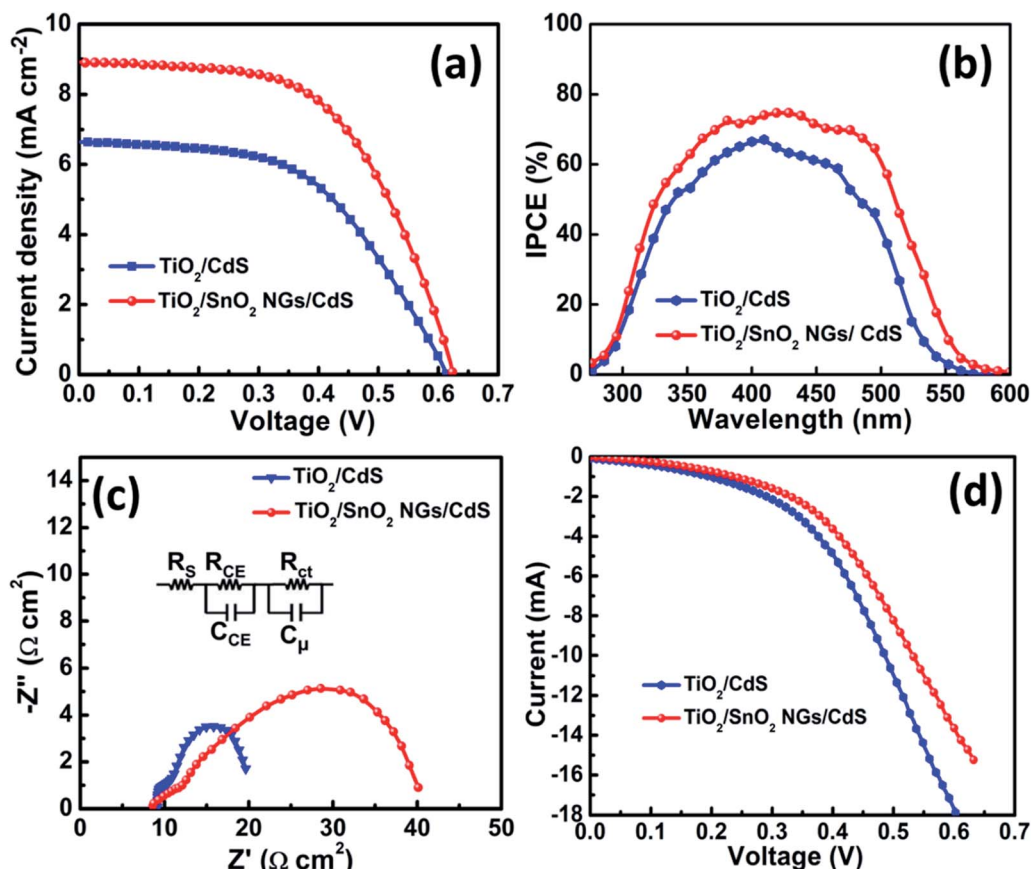


Fig. 6 (a)  $J-V$ , (b) IPCE and (c) EIS profiles of QDSSCs based on  $\text{TiO}_2/\text{CdS}$  and  $\text{TiO}_2/\text{SnO}_2$  NG/CdS photoelectrodes. (d)  $J-V$  profiles of QDSSCs under dark current.



**Table 1** Photovoltaic parameters of the as-prepared QDSSCs based on  $\text{TiO}_2/\text{CdS}$  and  $\text{TiO}_2/\text{SnO}_2$  NG/CdS photoelectrodes under one sun illumination

Cell	$V_{\text{OC}}$ (V)	$J_{\text{SC}}$ ( $\text{mA cm}^{-2}$ )	FF	PCE%	$R_{\text{ct}}$ ( $\Omega$ )	$C_{\mu}$ ( $\mu\text{F}$ )	$\tau_{\text{e}}$ (ms)
$\text{TiO}_2/\text{CdS}$	0.614	6.64	0.530	2.16	8.78	1358	11.92
$\text{TiO}_2/\text{SnO}_2$ NG/CdS	0.619	8.92	0.570	3.15	27.94	2183	60.99

phase is zero. The recombination resistance ( $R_{\text{ct}}$ ) at the  $\text{TiO}_2/\text{QD}$ /electrolyte interface and the chemical capacitance ( $C_{\mu}$ ) indexed to the bigger semicircle which is obtained at mid/low frequency.<sup>24,25</sup> Based on the equivalent circuit model (inset of Fig. 6c) and using Z-view software, the Nyquist plots were fitted to obtain the  $R_{\text{ct}}$  values and the fitting results are summarized in Table 1. There is no considerable change in the  $R_{\text{CE}}$ , which is due to the usage of similar electrolyte and counter electrode in the fabrication of QDSSCs. However,  $R_{\text{ct}}$  of the  $\text{TiO}_2/\text{SnO}_2$  NG/CdS based QDSSC ( $27.94 \Omega \text{ cm}^2$ ) is much higher than that of the  $\text{TiO}_2/\text{CdS}$  ( $8.78 \Omega \text{ cm}^2$ ). The higher  $R_{\text{ct}}$  of the  $\text{TiO}_2/\text{SnO}_2$  NG/CdS based QDSSC demonstrates that the growth of  $\text{SnO}_2$  NG over the  $\text{TiO}_2$  surface successfully suppresses the electron recombination at the  $\text{TiO}_2/\text{QDs}/\text{electrolyte}$  interfaces.<sup>24</sup> Hence,

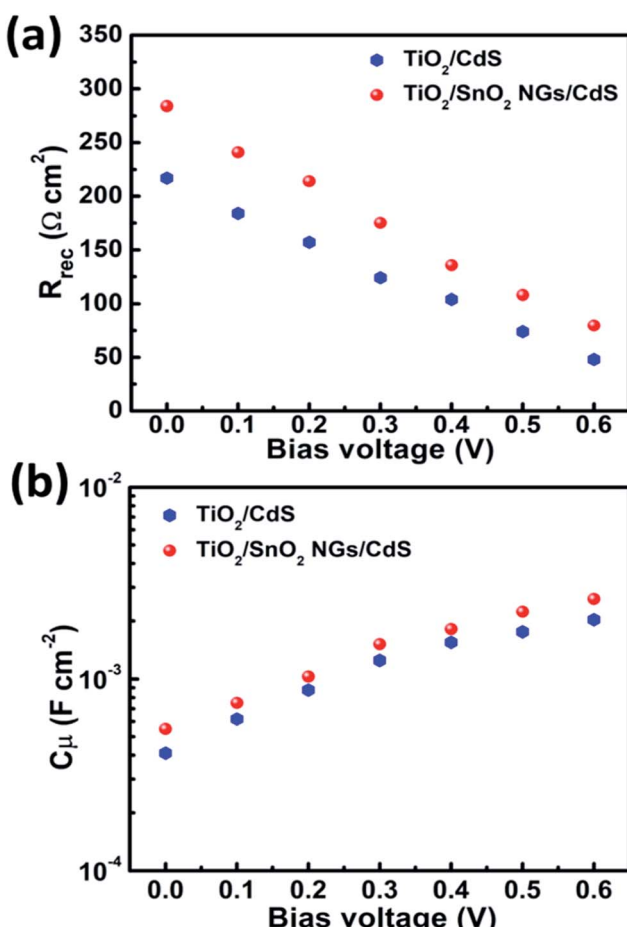
the growth of  $\text{SnO}_2$  NG interlayer hinders the interfacial charge recombination and enhances the photovoltaic performance ( $J_{\text{SC}}$  and FF). Moreover, QDSSC based on  $\text{TiO}_2/\text{SnO}_2$  NG/CdS photoelectrode achieves higher  $C_{\mu}$  ( $2183 \mu\text{F}$ ) than that of the  $\text{TiO}_2/\text{CdS}$  ( $1358 \mu\text{F}$ ) system. The higher  $C_{\mu}$  of the  $\text{TiO}_2/\text{SnO}_2$  NG/CdS system demonstrates the improved collection of photo-excited electrons into the conduction band of photoanode, which is mainly due to the hindered recombination at the  $\text{TiO}_2/\text{QDs}/\text{electrolyte}$  interfaces. Further, the electron life time ( $\tau_{\text{e}}$ ) of the QDSSCs can be obtained using the following equation,<sup>26</sup>

$$\tau_{\text{e}} = R_{\text{ct}} \times C_{\mu} \quad (1)$$

Interestingly, the  $\tau_{\text{e}}$  of the  $\text{TiO}_2/\text{CdS}$  with  $\text{SnO}_2$  NG interlayer (60.99 ms) is much higher than that of the  $\text{SnO}_2$  NG-free device (11.92 ms), which reveals the higher charge collection efficiency of the  $\text{TiO}_2/\text{SnO}_2$  NG/CdS system.

Under the dark condition, the  $J$ - $V$  plots of the  $\text{TiO}_2/\text{CdS}$  and  $\text{TiO}_2/\text{SnO}_2$  NG/CdS based QDSSCs were obtained and are shown in Fig. 6d. The electron recombination occurs at the interfaces of  $\text{TiO}_2/\text{QDs}$  and  $\text{TiO}_2/\text{electrolyte}$ , and this is the source of dark current.<sup>27</sup> Hence, a dark current study is a useful indicator of charge recombination. With the introduction of  $\text{SnO}_2$  NG interlayer, the  $\text{TiO}_2/\text{SnO}_2$  NG/CdS device delivers the reduced dark current, which is lower compared with that of the  $\text{TiO}_2/\text{CdS}$  device. The reduction of the dark current arose from an enhancement in electron transport with decreasing the internal resistance. As a result, the electron recombination was effectively reduced by the introduction of the  $\text{SnO}_2$  NG interlayer, and this contributed to the enhanced current and decreased electron loss.

Furthermore, to investigate the impact of  $\text{SnO}_2$  NG interlayer on the performance of QDSSCs, EIS tests were conducted at various bias applied voltages under dark condition in the 500 kHz to 100 mHz frequency range. The obtained recombination resistance ( $R_{\text{rec}}$ ) and chemical capacitance ( $C_{\mu}$ ) from the corresponding EIS tests are depicted in Fig. 7a and b, respectively. The  $R_{\text{rec}}$  and  $C_{\mu}$  reveal that the charge recombination process occurs at the  $\text{TiO}_2/\text{QDs}/\text{electrolyte}$  interfaces. A higher  $R_{\text{rec}}$  represents the low recombination rate and greater  $C_{\mu}$  values denote the Fermi level upward shift, yielding the enhanced  $V_{\text{OC}}$ .<sup>16</sup> It can be seen from Fig. 6a that the  $R_{\text{rec}}$  values of both devices decrease with the increment of the forward bias voltage due to the increased Fermi level of  $\text{TiO}_2$  at the forward bias. Also,  $\text{TiO}_2/\text{SnO}_2$  NG/CdS QDSSCs exhibits higher  $R_{\text{rec}}$  values than the  $\text{TiO}_2/\text{CdS}$  device under identical bias voltages. The recombination rate is inversely proportional  $R_{\text{rec}}$ .<sup>13</sup> Moreover, the higher  $C_{\mu}$  values of the  $\text{TiO}_2/\text{SnO}_2$  NG/CdS device denote the

**Fig. 7** EIS (a) recombination resistance ( $R_{\text{rec}}$ ) and (b) chemical capacitance ( $C_{\mu}$ ) at various forward bias voltages (V).

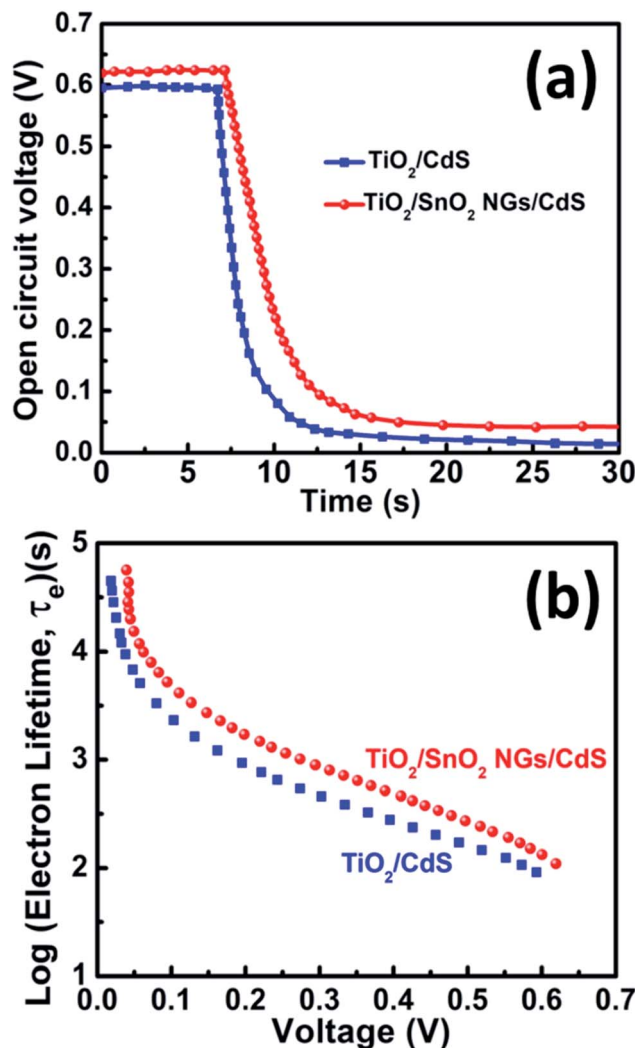


Fig. 8 (a)  $V_{OC}$  decay profiles of  $\text{TiO}_2/\text{CdS}$  and  $\text{TiO}_2/\text{SnO}_2 \text{ NG/CdS}$  QDSSCs. (b) Electron life time (in log-linear notation) obtained from  $V_{OC}$  decay measurements.

upward shift of the Fermi level of  $\text{TiO}_2$ , resulting in large  $V_{OC}$ . These EIS studies reveal the reduced recombination rate for the  $\text{TiO}_2/\text{SnO}_2 \text{ NG/CdS}$  device, which is favorable for the improved  $J_{SC}$  and FF.

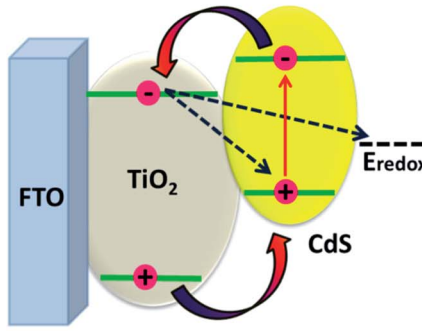
The excited electrons life time was examined using the open-circuit voltage ( $V_{OC}$ ) decay studies with time. Initially, the QDSSCs were irradiated with one sun illumination to a steady voltage, then the illumination was turned off and the  $V_{OC}$  decay data was obtained. Fig. 8a depicts the  $V_{OC}$  decay profiles of the  $\text{TiO}_2/\text{CdS}$  and  $\text{TiO}_2/\text{SnO}_2 \text{ NG/CdS}$  based QDSSCs. The  $V_{OC}$  decay plots clearly exhibit the continued monitoring of  $V_{OC}$  values under illumination and approach to decay after switching off the illumination. It is evident from the  $V_{OC}$  decay plots that the  $\text{TiO}_2/\text{SnO}_2 \text{ NG/CdS}$  based QDSSCs exhibit a slower voltage decay rate than the  $\text{TiO}_2/\text{CdS}$  photoanode. This behavior is mainly attributed to the  $\text{SnO}_2$  NG interlayer which efficiently suppresses the charge recombination at the  $\text{TiO}_2/\text{QDs}/$  electrolyte interfaces and also promotes the efficient electron transfer. Further, the electron life time ( $\tau_e$ ) can be estimated using the following equation:<sup>28</sup>

$$\tau_e = -\left(\frac{k_B T}{e}\right) \left(\frac{dV_{OC}}{dt}\right)^{-1} \quad (2)$$

where,  $k_B$ ,  $T$  and  $e$  have their usual meanings. Fig. 8b displays the plot of electron life time ( $\tau_e$ , in log sign) as a function of  $V_{OC}$ .<sup>29</sup> The  $\text{TiO}_2/\text{SnO}_2 \text{ NG/CdS}$  based QDSSCs deliver longer  $\tau_e$  values than that of  $\text{TiO}_2/\text{CdS}$ , implying a suppressed recombination of the photo-generated electrons leading to the efficient charge transfer, which agrees well with the EIS analysis.

Fig. 9 depicts the impact of the  $\text{SnO}_2$  NG interlayer on the charge transfer mechanism in QDSSCs. As shown in Fig. 9a, upon illumination, CdS captures the photons and produces the electron-hole pairs, named excitons. Then the electrons transfer into  $\text{TiO}_2$  conduction band, while the holes are reduced by polysulfide electrolyte. Simultaneously, the possibility of charge recombination also takes place at the interfaces of  $\text{TiO}_2/\text{CdS}$  QDs/electrolyte, which results in poor photovoltaic performance (Fig. 9a). Hence,  $\text{SnO}_2$  NG interlayer was introduced between the

(a)  $\text{TiO}_2/\text{CdS}$



(b)  $\text{TiO}_2/\text{SnO}_2 \text{ NGs/CdS}$

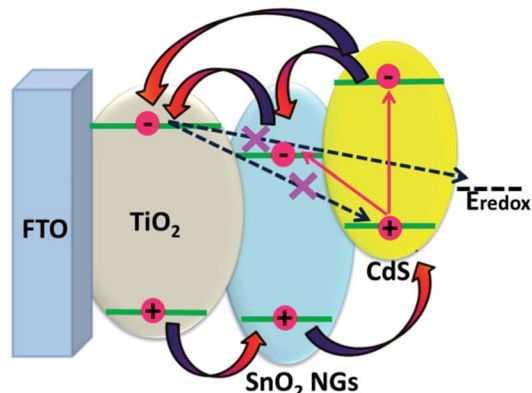


Fig. 9 Schematic demonstration of the charge transfer pathways in (a)  $\text{TiO}_2/\text{CdS}$  and (b)  $\text{TiO}_2/\text{SnO}_2 \text{ NG/CdS}$  based QDSSCs.

TiO<sub>2</sub> and CdS QDs (TiO<sub>2</sub>/SnO<sub>2</sub> NG/CdS) to prevent the charge recombination (Fig. 9b). The introduction of SnO<sub>2</sub> NG interlayer on TiO<sub>2</sub> surface retards the back injection of the electron from TiO<sub>2</sub> to QDs and also prevents the injection of excited electron from TiO<sub>2</sub> to redox couple, resulting in the high photovoltaic performance. Therefore, introducing SnO<sub>2</sub> NG interlayer over the TiO<sub>2</sub> surface achieves the outstanding properties, such as wide solar light-harvesting ability, enhanced charge transfer and suppressed charge recombination at the TiO<sub>2</sub>/QDs/electrolyte interfaces.

## 4. Conclusions

In summary, the introduction of SnO<sub>2</sub> NG layer between the TiO<sub>2</sub> and CdS QDs achieved the higher light-harvesting ability, improved charge transport and suppressed charge recombination at the TiO<sub>2</sub>/QDs/electrolyte interfaces. Evident from the *J*-*V*, EIS, IPCE, *V*<sub>OC</sub> decay and dark current measurements indicate that the photovoltaic properties of the TiO<sub>2</sub>/CdS QDSSCs were drastically enhanced after the deposition of SnO<sub>2</sub> NG layer due to the improved light absorption, fast charge transfer, reduced charge recombination and prolonged electron life time. Hence, the introduction of SnO<sub>2</sub> NG interlayer could be a favorable and effective approach to considerably improve the performance of QDSSCs. As a result, TiO<sub>2</sub>/SnO<sub>2</sub> NG/CdS based QDSSCs achieved the PCE (3.15%), *V*<sub>OC</sub> (0.619 V), *J*<sub>SC</sub> (8.92 mA cm<sup>-2</sup>), and FF (0.570), respectively, which are superior to TiO<sub>2</sub>/CdS device (PCE = 2.16%, *V*<sub>OC</sub> = 0.614 V, *J*<sub>SC</sub> = 6.64 mA cm<sup>-2</sup>, and FF = 0.530).

## Conflicts of interest

The authors declare no competing financial interest.

## Acknowledgements

This work was supported by UAEU Program for Advanced Research (UPAR) under grant no. 31S312. Also, this work was supported by BK 21 PLUS, Creative Human Resource Development Program for IT Convergence, Pusan National University, Busan, South Korea.

## References

- 1 W. Li and X. Zhong, *J. Phys. Chem. Lett.*, 2015, **6**, 796–806.
- 2 A. J. Nozik, M. C. Beard, J. M. Luther, M. Law, R. J. Ellingson and J. C. Johnson, *Chem. Rev.*, 2010, **110**, 6873–6890.
- 3 M. Ye, X. Gao, X. Hong, Q. Liu, C. He, X. Liu and C. Lin, *Sustainable Energy Fuels*, 2017, **1**, 1217–1231.
- 4 Z. Y. Yang, J. Z. Fan, A. H. Proppe, F. P. Arquer, D. Rossouw, O. Voznyy, X. Z. Lan, M. Liu, G. Walters, R. Q. Bermudez, B. Sun, S. Hoogland, G. A. Botton, S. O. Kelley and E. H. Sargent, *Nat. Commun.*, 2017, **8**, 1325.
- 5 R. L. Wu, T. Y. Wang, M. Wu, Y. B. Lv, X. P. Liu, J. J. Li, H. B. Shen and L. S. Li, *Chem. Eng. J.*, 2018, **348**, 447–454.
- 6 H. J. Kim, S. W. Kim, C. V. V. M. Gopi, S. K. Kim, S. S. Rao and M. S. Jeong, *J. Power Sources*, 2014, **268**, 163–170.
- 7 M. P. A. Muthalif, C. D. Sunesh and Y. Choe, *Appl. Surf. Sci.*, 2018, **440**, 1022–1026.
- 8 P. Subramanyam, P. Ghosal, M. Deepa and C. Subrahmanyam, *Electrochim. Acta*, 2018, **278**, 374–384.
- 9 W. Wang, W. L. Feng, J. Du, W. N. Xue, L. L. Zhang, L. L. Zhao, Y. Li and X. H. Zhong, *Adv. Mater.*, 2018, **30**, 1705746.
- 10 C. V. V. M. Gopi, M. V. Haritha, S. K. Kim and H. J. Kim, *Nanoscale*, 2015, **7**, 12552–12563.
- 11 F. Huang, Q. Zhang, B. Xu, J. Hou, Y. Wang, R. C. Masse, S. Peng, J. Liu and G. Cao, *J. Mater. Chem.*, 2016, **4**, 14773–14780.
- 12 C. V. V. M. Gopi, M. V. Haritha, H. Seo, S. Singh, S. K. Kim, M. Shiratani and H. J. Kim, *Dalton Trans.*, 2016, **45**, 8447–8457.
- 13 Z. Ren, J. Wang, Z. Pan, K. Zhao, H. Zhang, Y. Li, Y. Zhao, I. M. Sero, J. Bisquert and X. Zhong, *Chem. Mater.*, 2015, **27**, 8398–8405.
- 14 J. M. Li, *CrystEngComm*, 2017, **19**, 32–39.
- 15 Y. S. Lee, C. V. V. M. Gopi, M. V. Haritha and H. J. Kim, *Dalton Trans.*, 2016, **45**, 12914–12923.
- 16 Z. Du, H. Zhang, H. Bao and X. Zhong, *J. Mater. Chem. A*, 2014, **2**, 13033–13040.
- 17 S. Ozu, Y. Zhang, H. Yasuda, Y. Kitabatake, T. Toyoda, M. Hirata, K. Yoshino, K. Katayama, S. Hayase and R. Wang, *Front. Energy Res.*, 2019, **7**, 11.
- 18 E. N. Jayaweera, G. R. A. Kumara, C. Kumarage, S. K. Ranasinghe, R. M. G. Rajapakse, H. M. N. Bandara, O. A. Ileperuma and B. S. Dassanayake, *J. Photochem. Photobiol. A*, 2018, **364**, 109–115.
- 19 C. V. V. M. Gopi, M. V. Haritha, S. K. Kim, S. S. Rao, D. Punnoose and H. J. Kim, *RSC Adv.*, 2015, **5**, 2963–2967.
- 20 G. E. Patil, D. D. Kajale, V. B. Gaikwad and G. H. Jain, *Int. Nano Lett.*, 2012, **2**, 1–5.
- 21 A. Ray, A. Roy, P. Sadhukhan, S. R. Chowdhury, P. Maji, S. K. Bhattacharya and S. Das, *Appl. Surf. Sci.*, 2018, **443**, 581–591.
- 22 D. Wang, M. Zhang, Z. Chen, H. Li, A. Chen, X. Wang and J. Yang, *Sens. Actuators, B*, 2017, **250**, 533–542.
- 23 A. Hodaei, A. S. Dezfuli and H. R. Naderi, *J. Mater. Sci.: Mater. Electron.*, 2018, **29**, 14596–14604.
- 24 F. Huang, J. Hou, Q. Zhang, Y. Wang, R. C. Massé, S. L. Peng, H. L. Wang, J. S. Liu and G. Z. Cao, *Nano Energy*, 2016, **26**, 114–122.
- 25 R. Zhou, Q. F. Zhang, E. Uchaker, J. Lan, M. Yin and G. Z. Cao, *J. Mater. Chem. A*, 2014, **2**, 2517–2525.
- 26 H. Kim, G. Xu, C. V. V. M. Gopi, H. Seo, M. V. Haritha and M. Shiratani, *J. Electroanal. Chem.*, 2017, **788**, 131–136.
- 27 J. Bisquert, A. Zaban, M. Greenshtein and I. M. Seró, *J. Am. Chem. Soc.*, 2004, **126**, 13550–13559.
- 28 S. B. Ambade, R. B. Ambade, R. S. Mane, G. W. Lee, S. F. Shaikh, S. A. Patil, O. S. Joo, S. H. Han and S. H. Lee, *Chem. Commun.*, 2013, **49**, 2921–2923.
- 29 H. Seo, D. Ichida, S. Hashimoto, N. Itagaki, K. Koga, M. Shiratani, S. H. Nam and J. H. Boo, *J. Nanosci. Nanotechnol.*, 2016, **16**, 4875–4879.

